Proceedings of ASME Turbo Expo 2011
GT2011
June 6-10, 2011, Vancouver, British Columbia, Canada

GT2011-45396

PERFORMANCE EVALUATION OF AN UNSTEADY TURBINE DRIVEN BY A PULSED DETONATION COMBUSTOR

Kurt P. Rouser
Air Force Institute of Technology
Wright-Patterson AFB, OH, USA

Paul I. King
Air Force Institute of Technology
Wright-Patterson AFB, OH, USA

Frederick R. Schauer
Air Force Research Laboratory
Wright-Patterson AFB, OH, USA

Rolf Sondergaard
Air Force Research Laboratory
Wright-Patterson AFB, OH, USA

John L. Hoke
Innovative Scientific Solutions, Inc.
Dayton, OH, USA

ABSTRACT

Replacing a Brayton cycle near constant-pressure combustor with a pulsed detonation combustor (PDC) may take advantage of potential performance improvements from low-entropy, pressure-gain heat addition. In this paper, the radial turbine of a Garrett automotive turbocharger is coupled to a hydrogen fueled PDC. Unsteady turbine power is obtained with a conventional dynamometer technique. Sampling frequencies greater than 10 kHz resolve rapid flowfield transients of confined detonations which occur in less than a millisecond and include peak gas pressures exceeding 4 MPa and peak gas temperatures greater than 2,400 K. Results include 6 ms time histories of turbine inlet and exit temperature, pressure, mass flow, and enthalpy during blowdown of a PDC. The unsteady inlet flowfield included momentary reverse flow, which was not observed at the turbine exit. Full pulsed detonation cycle time histories of turbine power, rotor speed, rotational energy and net shaft torque are included to describe the turbine response to detonations. Rotor speed is periodic and net shaft torque oscillates in response to a detonation. Results are shown for fill fractions ranging from 0.5 to 1.0 with a 0.5 purge fraction. PDC operating frequencies in this study range from 10 Hz to 25 Hz.

INTRODUCTION

Over the past decade, there has been a growing interest in turbines driven by pressure gain combustion. Incorporating pressure gain combustion into a conventional Brayton cycle gas may lower entropy associated with heat addition and increase thermal efficiency. The pulsed detonation combustion process, in particular, is characterized by a significant pressure rise and lower entropy production than steady deflagration combustion.

Heiser and Pratt [1] proposed that the ideal Humphrey cycle may be considered a modification to the ideal Brayton cycle, replacing constant-pressure combustion with constant-volume combustion. They showed that the ideal Humphrey cycle enjoys a significant cycle thermal efficiency advantage over the ideal Brayton cycle for cycle static temperature ratios between one and three, but they also determined that the advantage diminished rapidly for cycle static temperature ratios greater than three. Because a pulsed detonation combustor (PDC) operates with near constant-volume heat addition, the ideal Humphrey cycle may represent the upper theoretical limit for hybrid pulsed detonation turbine engines. Heiser and Pratt [1], Bussing and Pappas [2], and Dyer and Kaemming [3] have characterized the theoretical performance improvement of a pulse detonation engine (PDE) cycle; however, there has been little experimental work that demonstrates the performance advantage of a detonation driven turbine.

Dyer and Kaemming [3] analyzed the thermodynamic basis of detonation engines for aircraft. Their ideal cycle thermal efficiency for a detonation driven cycle was greater than that for a deflagration driven Brayton cycle. Although the advantage diminished with increasing flight Mach number, PDE thermal efficiency remained higher due to lower Rayleigh losses associated with heat addition by detonation combustion.

Integrating detonation combustion into a gas turbine engine offers the potential for a hybrid PDE-Brayton cycle to approach the ideal thermal efficiency of a PDE.

In 2002 and 2003, at the Air Force Research Laboratory (AFRL), Hoke, et al. [4] and Schauer, et al. [5] experimentally demonstrated the feasibility of PDC coupled to a radial turbine of an automotive turbocharger, accumulating more than 50,000 detonations through the turbine and sustaining a 25 minute continuous run. However, the thermal efficiency of this arrangement was low (less than 7%).

Between 2006 and 2008, at the University of Cincinnati (UC), Glaser, et al. [6] and Caldwell, et al. [7, 8] integrated a dual-stream axial turbine with an array of PDC tubes, in which detonation exhaust mixed with steady bypass air before entering the turbine. Power was measured with a dynamometer. A bypass ratio of eight allowed for use of traditional instrumentation methods to assess turbine efficiency. The UC experimental comparison of steady deflagration and pulsed detonation did not show an improvement in turbine power or efficiency; however, subsequent work indicated that the cause may have been due to shock-jet interaction between the detonation exhaust and the steady bypass stream resulting in a vortex that caused viscous mixing of the turbine inlet flow, dissipating work available for power extraction.

In 2010, at AFRL, Rouser, et al. [9] demonstrated a significant increase in average specific work with a full-admission radial turbine driven by a pulsed detonation combustor. A comparison made to a steady deflagration combustor at similar combustor inlet conditions showed a corresponding 27% decrease in average specific fuel consumption. Ensuing research by Rouser, et al. [10] showed a trend toward quasi-steady rotor speed with increasing PDC frequency.

Evaluating the details of unsteady performance requires time-accurate measurements of pressure, temperature, and velocity. Transients associated with detonation combustion require minimum sampling frequencies of 10 kHz and the capability to measure peak pressures over 4 MPa and peak temperatures over 2,400 K. The objective of the current research is to evaluate characteristics of unsteady turbine performance, including time-accurate rotor speed and net shaft torque response.

PULSED DETONATION CYCLE

The pulsed detonation cycle is characterized by three major phases: fill, fire and purge, as shown in Fig. 1. The duration of each phase may differ from the others, limited by physical constraints associated with each. For example, the duration of the fill phase is limited by the amount of time required to fill the volume, which is affected by chamber geometry, inlet manifold pressure, inlet valve type, etc. The fire phase is divided into four events: ignition, deflagration to detonation transition (DDT), detonation, and blowdown. The duration of these events is also constrained by various physical parameters such as fuel type and equivalence ratio, ignition source, DDT devices and chamber geometry. The purge phase acts as a buffer between fire and fill phases, evacuating high temperature exhaust products and cooling chamber walls. The duration of the purge phase is constrained by physical parameters similar to that of the fire phase, as well as by cycle operability limits. Limits on cycle operating frequency depend on duration of each phase.

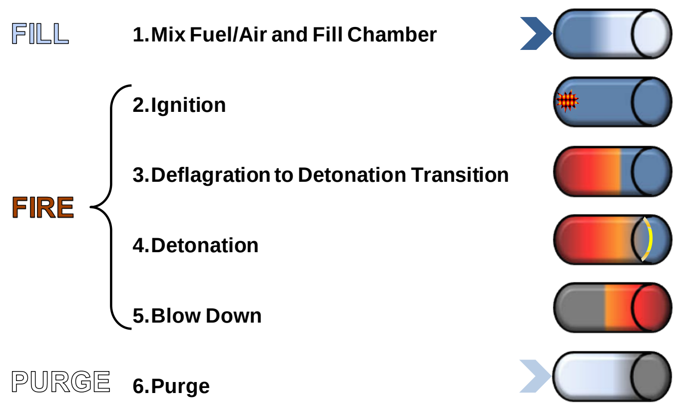

Figure 1. PULSED DETONATION CYCLE.

Even at operating frequencies as low as 10 Hz, the pulsed detonation cycle is dynamic. Each phase is only a few milliseconds long, and transients during each phase occur even faster than that. For example, a detonation wave in hydrogen propagates at about Mach 5 and is closely coupled to a preceding, mutually supporting shock. High-frequency instrumentation must have a minimum sampling rate of 10 kHz to achieve sufficient waveform resolution of the fastest transient events in the pulsed detonation flow, which occur in less than a millisecond. Instrumentation must also have a high operating range to capture peak temperatures and pressures associated with a detonation.

Pulsed Detonation Cycle Coupled to a Gas Turbine

Rouser, et al. [9] demonstrated the advantage of pulsed detonation driven turbines over steady deflagration driven turbines. A comparison was made by coupling the radial turbine of an automotive turbocharger to a pulsed detonation combustor, using an arrangement similar to this current study as described later. The same turbine was also coupled to an approximately constant pressure combustor (CPC) with steady deflagration operation. At combustor inlet total pressure ratios of about two, there was more than 40% improvement in average specific work for the PDC turbine. Figure 2 shows a time history of power and rotor speed for two detonation cycles at 11 Hz operation. Power was obtained using a compressor dynamometer similar and was higher at nearly every instant with the detonation driven turbine than with the steady CPC driven turbine (dashed line).

Rouser, et al. [9], determined that the initial rise in rotor speed coincides with detonation arrival at the turbine. Rotor speed continues to climb during the start of blowdown. As blowdown progresses, combustion chamber pressure drops to sub-ambient and rotor speed begins to fall. Rotor speed continues to drop during the purge phase, as combustion chamber pressure equalizes to ambient, and then levels during the fill phase, as combustion chamber pressure begins to rise once again.

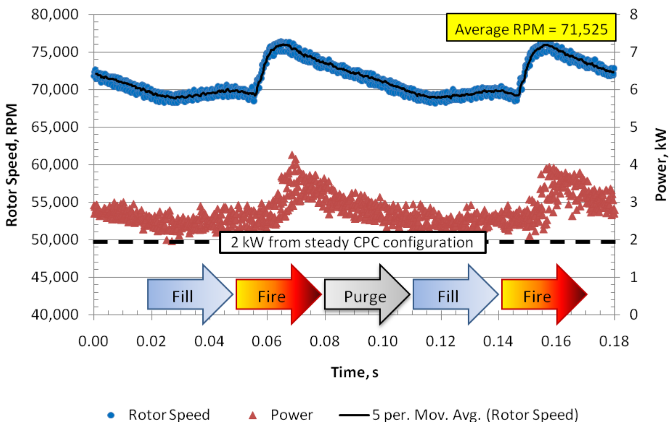

Figure 2. DETONATION DRIVEN TURBINE POWER AND ROTOR SPEED OVER TWO PDC CYCLES AT 11 HZ [9].

Subsequently, Rouser, et al. [10] revealed the influence of PDC frequency on rotor speed, using the same speed instrumentation as the current research, which is described later. Figure 3 shows rotor speed for three different frequencies. Instantaneous rotor speed is normalized by peak rotor speed, and time is normalized by cycle time. As PDC frequency increases, rotor spin-down decreases, approaching a quasi-steady response. However, at each frequency, there is a sharp acceleration from the end of one cycle and the start of the next.

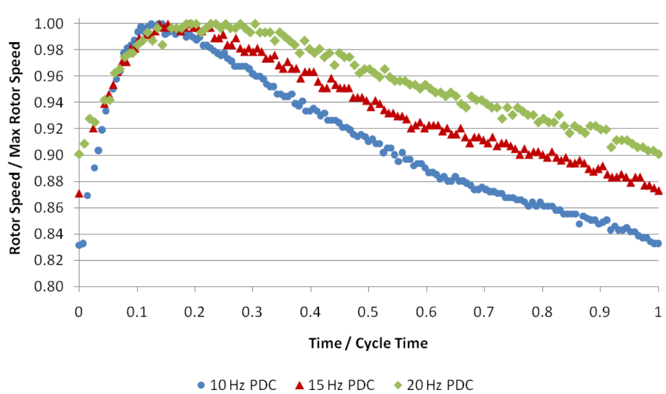

Figure 3. ROTOR SPEED RESPONSE TO 10, 15, AND 20 HZ PDC OPERATING FREQUENCIES [10].

EXPERIMENTAL SET-UP

Experiments in this current study were carried out in the AFRL Detonation Engine Research Facility (DERF), depicted schematically in Fig. 4. The facility supplies compressed air to the main fill and purge manifolds. Hydrogen is added to the main manifold to achieve a desired hydrogen-air mixture (ϕ = 1.0 in these experiments). Each air and fuel stream is controlled by Tescom electromagnetic controllers that actuate pressure regulators that meter flow through calibrated, choked converging-diverging nozzles. Fill and purge distribution is done by an automotive engine head, in which a cam operates intake and exhaust valves at desired PDC frequencies. Intake valves open for the main fill mixture, and exhaust valves open to inject purge air. During the fire phase, intake and exhaust valves are closed. Ignition timing is based on the cam design, with a variable spark delay for optimal operability. Duration of the three PDC phases was equal in these experiments.

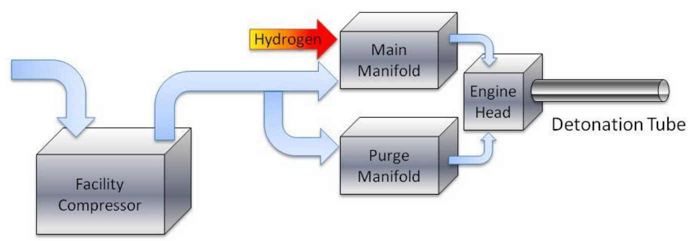

Figure 4. DIAGRAM OF THE AFRL DETONATION ENGINE RESEARCH FACILITY.

Pulsed Detonation Combustor

The pulsed detonation combustor consisted of three sections of schedule-40 steel pipe, depicted in Fig. 5. The first section was a 26.6 mm diameter pipe, 305 mm in length, and coupled to the engine head. The second section was a 40.8 mm diameter pipe, 915 mm in length, and coupled to the first pipe with a reducer. The final section was a 52.5 mm diameter pipe, 152 mm in length, and coupled to the second pipe with a reducer. The exit of the final pipe section transitioned from round to rectangular and was welded to a T3 turbocharger flange. The total combustor length was 1.4 m, and the volume was 0.0019 m^3. There were no internal DDT obstacles or devices. Such devices would reduce the amount of pressure gain from combustion. Ignition was accomplished with a pre-detonator.

The diameter of the first combustor section was chosen to ensure that the detonation from the pre-detonator was re-established. The diameter of the third combustor section was chosen to match the T3 inlet circumference. The diameter of the second combustor section was chosen to ensure a smooth transition between the first and third sections.

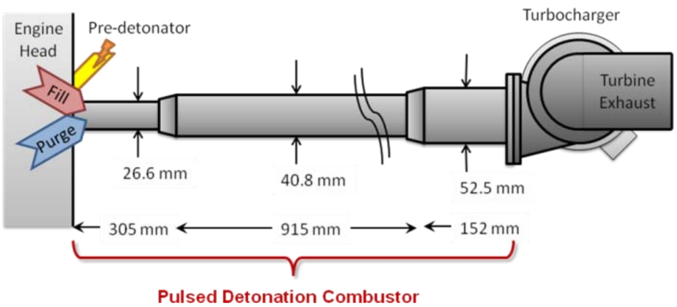

Figure 5. PULSED DETONATION COMBUSTOR AND TURBOCHARGER EXPERIMENTAL ARRANGEMENT.

The pre-detonator, pictured in Fig. 6, consisted of a 14 mm tube with an internal spiral for DDT. The tube was contained in a water jacket for cooling. Propane and nitrous oxide were the pre-detonator fuel and oxidizer, respectively, and an automotive spark plug was the ignition source. A detonation was established in the pre-detonator tube and then passed into the pulsed detonation combustor.

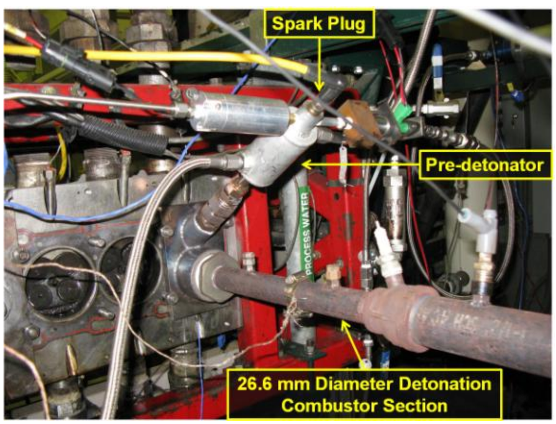

Figure 6. PRE-DETONATOR AND PULSED DETONATION COMBUSTOR ARRANGMENT AT THE ENGINE HEAD.

PDC operation was attained by first setting fill and purge air flow at a desired operating frequency via cam speed. At that point, pre-detonator operation was started, and hydrogen was added to the main fill manifold to achieve a stoichiometric fuel-air ratio. Typically, the desired fuel-air ratio was achieved within five seconds, during which time intermittent detonations occurred. Once the start-up sequence was complete and stoichiometric operation was achieved, data was taken and then fuel was shut-off. Most run times were less than 30 seconds.

Six ion probes were installed at 152 mm intervals along the length of the 40.8 mm diameter combustor section. The probes are modified automotive spark plugs. Ionized gas associated with a detonation front causes a short circuit in the spark plugs, indicating the arrival of the detonation flame front, and flame speed was determined from the transition time between probes. Detonations were confirmed by verifying Chapman-Jouguet (C-J) velocities had been achieved (approximately 1800 m/s for hydrogen-air at the operating conditions in this study).

In addition to operating frequency, two other key operating parameters for the PDC are fill fraction (FF) and purge fraction (PF). These volumetric fractions determine how much of the detonation tube is filled during the respective phases of the PDC cycle. For this study, the duration of fill and purge is equal and is determined by the operating frequency. The volumetric flow rate is governed by manifold pressure and mass flow.

$$FF = \frac{\left(\dot{\forall}_{air} + \dot{\forall}_{fuel}\right) \cdot t_{fill}}{\forall_{tube}} \tag{1}$$

$$PF = \frac{\left(\dot{\forall}_{air}\right) \cdot t_{purge}}{\forall_{tube}} \tag{2}$$

Ion probes at any location confirm FF for a certain desired fill fraction. When the fill volumetric flow rate is too low, a detonation is not detected by the ion probe associated with an FF location. Volumetric flow rate is adjusted until FF is confirmed. Mounting a turbocharger to the PDC generates back-pressure, which requires a higher volumetric flow rate than without the turbocharger.

Table 1 includes the range of operating conditions explored in this study. Total turbine airflow ranged from 1.6 kg/min to 5.1 kg/min as frequency increased from 10 Hz to 25 Hz and fill fraction increased from 0.5 to 1.0.

Table 1. PDC OPERATING CONDITIONS.

Frequency (Hz)	Fill Fraction	Purge Fraction	Fill Flow (kg/min)	Purge Flow (kg/min)	Fill Pressure (kPa)	Purge Pressure (kPa)	Manifold Temp (K)
10	0.5	0.5	0.65	0.93	113.51	115.75	296.55
10	0.6	0.5	0.78	0.94	117.21	116.68	296.55
10	0.7	0.5	0.91	0.94	121.42	117.83	296.55
10	0.8	0.5	1.06	0.94	126.28	117.99	296.55
15	0.5	0.5	0.99	1.41	131.63	223.28	296.55
15	0.6	0.5	1.19	1.41	138.23	233.64	296.55
15	0.7	0.5	1.39	1.41	145.10	234.14	296.55
15	0.8	0.5	1.58	1.41	152.13	241.31	296.55
15	1.0	0.5	2.96	2.11	82.74	103.91	301.93
20	0.5	0.5	1.33	1.88	139.89	147.38	293.71
20	0.6	0.5	1.59	1.88	149.92	148.92	293.71
20	0.7	0.5	1.86	1.88	159.51	149.85	293.71
20	0.8	0.5	2.11	1.88	167.43	150.90	293.71
25	0.5	0.5	1.68	2.36	150.91	199.48	293.99
25	0.6	0.5	2.01	2.36	162.92	200.34	293.99
25	0.7	0.5	2.33	2.36	172.54	203.43	293.99
25	0.8	0.5	2.66	2.35	184.68	203.05	293.99

Garrett Radial Turbine

A Garrett T3/T4E turbocharger, pictured in Fig. 7, was coupled to the PDC exit, as shown in Fig. 5. The turbine wastegate was capped so that all combustor exhaust passed through the turbine. A 77 mm diameter steel pipe elbow was attached to the turbine exhaust flange.

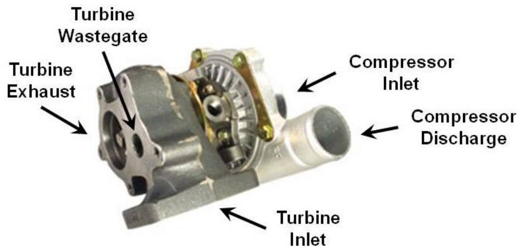

Figure 7. GARRETT T3/T4E TURBOCHARGER (USED WITH PERMISSION FROM ADVANCED TUNING PRODUCTS, INC.).

The T3/T4E turbocharger is equipped with an 11-blade, radial turbine and a 45-trim radial compressor having six primary impeller blades and six splitter blades. A water-cooled center housing, shown in Fig. 8, contains the shaft and bearing assembly. A journal bearing turbocharger was chosen for durability under detonation loads. According to the manufacturer, the rotating assembly has a moment of inertia of 3.2E-5 kg m^2 and a maximum turbine efficiency of 61%.

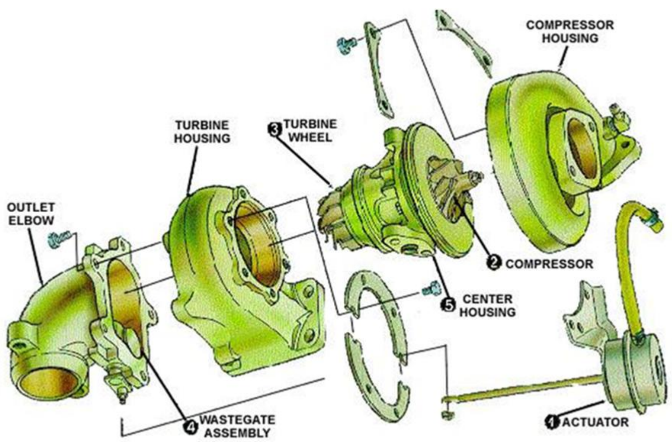

Figure 8. TURBOCHARGER ASSEMBLY (USED WITH PERMISSION FROM ADVANCED TUNING PRODUCTS, INC.).

INSTRUMENTATION

The measurement techniques employed in this research are well established methods, and each piece of instrumentation is expected to have low uncertainty error; however, there is little or no experimental data to date that may be used to confirm or calibrate magnitudes and response times. The detonation flowfield is known to be very non-uniform and dynamic with stochastic behavior. Furthermore, there is not a generally accepted set of formulations for unsteady turbine performance in a pulsed detonation operating environment. Therefore, confidence in the instrumentation is high, but confidence in the results is primarily based on analytical expectations and repeatability. Table 2 includes a summary of instrumentation used in this study.

Table 2. SUMMARY OF INSTRUMENTATION

Property	Instrumentation Type	Location	Sampling Frequency
$\dot{m}_{fill}$	Calibrated Converging-Diverging Nozzle	Facility Air Supply Line	1 Hz
$\dot{m}_{purge}$	Calibrated Converging-Diverging Nozzle	Facility Air Supply Line	1 Hz
$\dot{m}_{fuel}$	Calibrated Converging-Diverging Nozzle	Facility Fuel Supply Line	1 Hz
T_{wall}	J-Type Thermocouples	PDC Tubes and Turbocharger Compressor and Turbine Housings	1 Hz
T_{H_2O}	T-Type Thermocouples	Turbocharger Cooling Water Inlet and Exit	1 Hz
ω	Garrett Speed Sensor (Part Number 781328-0002)	Turbocharger Compressor Housing	1 MHz
$\dot{m}_{compr}$	Professional Flow Technologies Model 92 Special Mass Air Flow Sensor	304.8 mm Upstream of Turbocharger Compressor	1 MHz
$P_{compr,exit}$	Sensotec 344 kPa Static Pressure Transducer	1.17 m Downstream of Turbocharger Compressor	1 MHz
$P_{turb,inlet}$	5.17 MPa Kulite Pressure Transducer	25.4 mm Upstream of Turbine Inlet Flange	1 MHz
$P_{turb,exit}$	5.17 MPa Kulite Pressure Transducer	152 mm Downstream of Turbine	1 MHz
$T_{turb,inlet}$	Two-Band Optical Pyrometry with PCO Dimax High-Speed Color Camera	610 mm Upstream of Turbine Inlet Flange	11.484 kHz
$T_{turb,exit}$	Two-Band Optical Pyrometry with PCO Dimax High-Speed Color Camera	762 mm Downstream of Turbine	11.484 kHz
$V_{turb,inlet}$	Particle Streak Velocimetry with PCO Dimax High-Speed Color Camera	610 mm Upstream of Turbine Inlet Flange	14.925 kHz
$V_{turb,exit}$	Background Oriented Schlieren with Phantom v7 Camera	762 mm Downstream of Turbine Exit	14.925 kHz

The middle of each of the three combustor sections was instrumented with an external wall-mounted J-type thermocouple. J-type thermocouples were also attached externally to the turbine and compressor housings. T-type thermocouples were used to measure turbocharger center housing cooling water inflow and outflow temperatures. On every test run, thermocouple data was sampled once per second along with facility operating data using a low-speed data acquisition system which was apart from the high-speed system used for other turbocharger measurements.

Rotor Speed Instrumentation

A Garrett speed sensor (part number #781328-0002), pictured in Fig. 9, was mounted to the compressor housing to measure blade passing frequency. The sensor emits a magnetic field that is interrupted by passing blades. The sensor input frequency is one pulse per blade. The internal sensor electronics divide the input signal by eight, so that the output frequency is a square-wave signal at 1/8th the actual blade passing frequency. The output frequency was used to calculate rotor speed. Rotor speed data was sampled at 1 MHz. Calculations of net shaft torque and rotational energy were made using speed data and the rotating assembly moment of inertia, 3.2E-5 kg m^2.

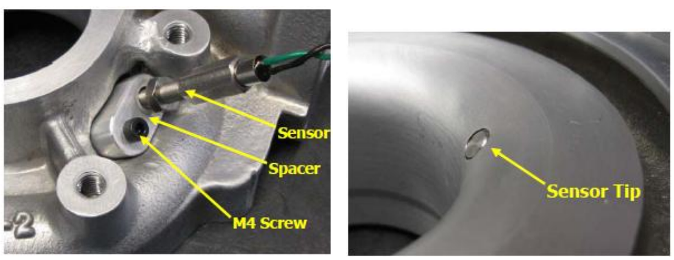

Figure 9. GARRETT SPEED SENSOR INSTALLED IN COMPRESSOR HOUSING.

Compressor Dynamometer

The turbocharger compressor was used as a dynamometer to measure power. A mass air flow (MAF) sensor (Professional Flow Technologies Model 92 Special) was mounted to the compressor inlet, as shown in Fig. 10, receiving ambient air. The compressor discharge was instrumented with a wall-mounted Sensotec 344 kPa static pressure transducer located 1.17 m downstream of the compressor exit along a 52.5 mm diameter pipe (not shown). A J-type thermocouple was located six inches downstream of the pressure transducer. A ball valve, located 609 mm downstream of the thermocouple, was used to back-pressure the compressor. The ball valve was set so that the compressor operated toward the center of its operating map. Several different compressor operating conditions were achieved by adjusting the PDC operating frequency and fill fraction and leaving the ball valve fixed.

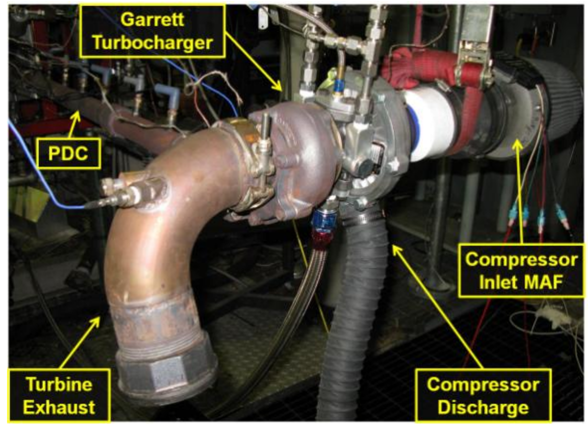

Figure 10. TURBOCHARGER MOUNTED TO THE PULSED DETONATION COMBUSTOR

Turbine Flow Instrumentation for Blowdown

Turbine inlet and exit pressures, temperatures, and velocities were measured on different test runs, under the same test set-up and operating conditions. Kulite static pressure transducers were mounted to the inlet and exhaust walls with a 14 mm stand-off for cooling. The inlet transducer was located 25.4 mm upstream of the T3 flange. The exit transducer was located 152 mm downstream of the turbine. The sampling frequency for pressures was 1 MHz. Inlet and exit pressure measurements were made simultaneously; however, they were made apart from velocity and temperature measurements.

For velocity and temperature optical instrumentation, a square pipe section with a 50.8 mm by 50.8 mm cross section, a 610 mm length, and two side-mounted quartz windows was added upstream of the turbocharger, coupled between the second and third combustor sections, as shown in Fig. 11. A similar arrangement with a polycarbonate window was mounted downstream of the turbo, coupled to the exhaust elbow with a pipe reducer.

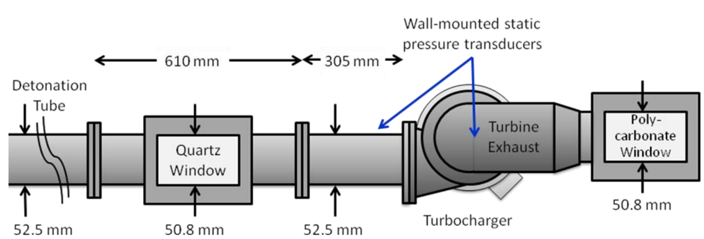

Figure 11. TURBINE FLOW INSTRUMENTATION EXPERIMENTAL ARRANGEMENT.

Silicon carbide (SiC) particles with a 2400 grit size were injected into the PDC fuel line with a standard dry cyclone seeder. A PCO Dimax high-speed color camera was used for two-band optical pyrometry, using the seed particles black body emission to determine static temperature at the turbine inlet and exit. The emission threshold was 1300 K, below which particle emission was insufficient to detect. Thus, pyrometry temperature data was not available during fill and purge phases. Inlet and exit temperature measurements were made on separate test runs and were synchronized by ignition timing.

Sampling frequency was set by optical pyrometry, the limits of which were determined by the desired resolution for a combination of picture size and pixel size. The minimum sampling frequency was 10 kHz to achieve sufficient time resolution of the fastest transient events in the pulsed detonation flow, which occur in less than a millisecond. The camera was set to a 1.5 μs exposure and 87 μs inter-frame time to achieve a frame rate of 11,484 frames/s.

Measurements with a tungsten lamp and spectrometer allowed the spectral responsivity of the red, green and blue channels of this camera to be measured. Substituting the spectral responses and integrating them with a blackbody function over the appropriate wavelengths allows the ratio to be determined as a function of temperature. Figure 12 shows a single pyrometry frame for a detonation passing into the turbine inlet. Streamwise centerline temperature is plotted alongside the pyrometry frame.

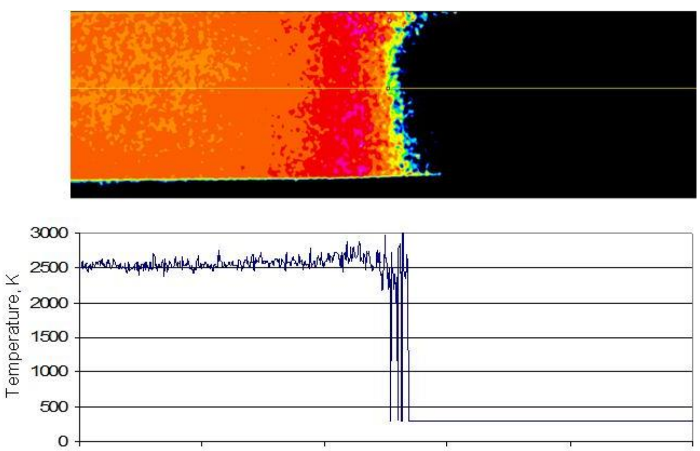

Figure 12. SINGLE PYROMETRY FRAME OF A DETONATION TRAVELLING FROM LEFT TO RIGHT AT THE TURBINE INLET. BLACK REPRESENTS UNBURNED FUEL-AIR.

The SiC particles were also used for particle streak velocimetry (PSV) measurements at the turbine inlet. By increasing exposure time of the PCO Dimax high-speed camera from 1 to 10 μs, time history of particle streaks were traced from frame to frame. The turbine inlet velocity field was determined by dividing the length of particle streaks by the exposure time. To increase the contrast between the soot streaks and the surrounding gas emission, an edge enhancing convolution was applied to images before analysis. Figure 13 shows a single frame of PSV before and after post-processing.

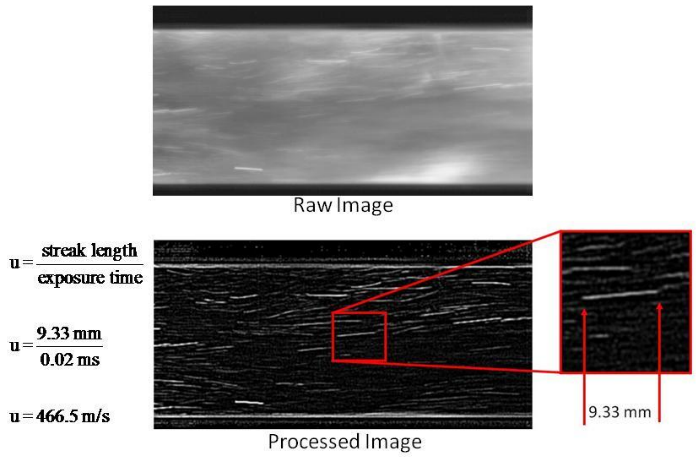

Figure 13. PARTICLE STREAK VELOCIMETRY IMAGE DURING BLOWDOWN AT THE TURBINE INLET.

Turbine exit velocity was obtained using background oriented Schlieren (BOS), an optical measurement technique that has the ability to visualize density gradients. BOS can be described as a simple Schlieren technique based on image displacements of a background caused by density gradients in the optical path. The background displacements are typically determined using particle image velocimetry (PIV) based correlation methods which are well established. The BOS technique was chosen for this study because of its ability to function with high speed cameras, which allow density field images of pulsed detonation exhaust to be captured at a very high rate. To achieve these high rates, a Phantom v7 was utilized in conjunction with an over-driven pulsed light-emitting diode (LED) array. High framing rates required that the BOS background be setup in a transmission mode with the LED array arranged as a back light. This arrangement ensured that the maximum amount of light was available to the Phantom camera, which helped to minimize the pulse width of the LED array (~1μs) and allowed the use of a large f# (22) needed for increased sensitivity and measurement resolution.

BOS experiments took place on separate test runs but under the same conditions as those for turbine inlet and exit pressures and temperatures, as well as for turbine inlet velocity. Figure 14 shows the experimental arrangement used to capture the BOS data. The output of the pulsed LED array was directed through a series of scattering glass plates that formed the random background needed for the BOS experiment. The background image from the scattering plate was recorded with a high speed cine Phantom v7 camera with a 500 ns exposure and 122 μs inter-frame time. Transient density gradients caused by the PDC-turbine exhaust pulse distorted the background image and were recorded by the Phantom camera. The displacement of the background due to the density field was determined by conducting a correlation analysis between the non-disturbed image (no flow) and the gradient disturbed images (flow). This is an established approach used in PIV analysis where particle movement between successive images is correlated to yield the velocity field. To accomplish this task, the displacement magnitude images were correlated (using PIV analysis software) to yield the gradient density velocity.

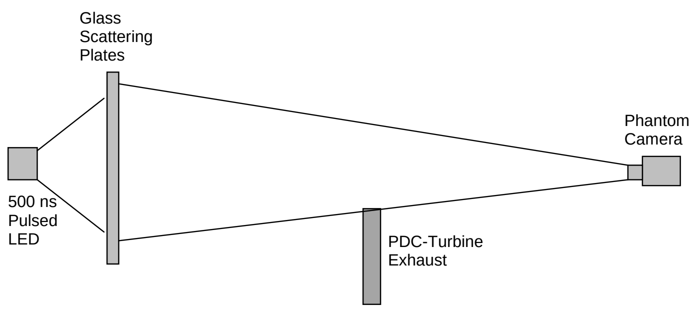

Figure 14. BACKGROUND ORIENTED SCHLIEREN ARRANGEMENT UTILIZED FOR HIGH-SPEED VISUALIZATION AND VELOCITY MEASUREMENTS AT THE TURBINE EXIT.

TURBINE PERFORMANCE EQUATIONS

Primary figures of merit are typically time-average specific work and time-average turbine efficiency. Additionally, time-resolved rotor speed, net shaft torque, and rotational kinetic energy are considered to evaluate turbine response to pulsed detonations.

Previous work explains the use of the turbocharger compressor dynamometer [9]. Equation 3 characterizes turbine specific work, relating turbine power to compressor power to enthalpy change across the compressor by including a term, $\overline{\eta}_{mech}$, for time-averaged mechanical losses. Typical values for turbocharger mechanical efficiency at high-power are above 95%. In this study, to compute specific work, mechanical efficiency was arbitrarily set to unity. Compressor power was related to change in total enthalpy across the compressor by including time-averaged compressor efficiency, $\overline{\eta}_{compr}$, which was determined from the manufacturer's compressor operating map.

$$W_s = \frac{\dot{W}_{turb}}{\dot{m}_{turb,in}} = \frac{\dfrac{\dot{W}_{compr}}{\overline{\eta}_{mech}}}{\dot{m}_{turb,in}} = \frac{\dfrac{\Delta H_{t,compr}}{\overline{\eta}_{mech}}}{\dot{m}_{turb,in}} = \frac{\dfrac{\Delta H_{t,compr,ideal}}{\overline{\eta}_{mech}\overline{\eta}_{compr}}}{\dot{m}_{turb,in}} \quad (3)$$

Ideal change in total enthalpy was calculated using compressor inlet mass flow, inlet total temperature, and inlet and exit total pressure. Pressures were used because of the transducer fast response to unsteady flow.

$$\Delta H_{t,compr,ideal} = \dot{m}_{compr,in} \cdot \overline{c}_p \cdot T_{t,compr,in} \left(\left(\frac{P_{t,compr,exit}}{P_{t,compr,in}} \right)^{\frac{\gamma-1}{\gamma}} - 1 \right) \quad (4)$$

Based on low turbocharger compressor mass flow rates, the compressor inlet and exit velocities were determined to be low subsonic. Therefore, total pressure and total temperature were taken to be approximately equal to measured static pressure and temperature, respectively. Compressor inlet mass flow was obtained from MAF measurements, and total turbine inlet mass flow was obtained from facility air flow into the main and purge manifolds, as described earlier.

Specific work was considered on a time-average basis in order to remove the effect of unsteady power stored in the shaft. As rotor speed accelerated, power was stored in the form of rotational energy and shaft twist. As rotor speed decelerated, the rotational energy and shaft twist decreased, reducing the storage of power. Over each PDC cycle, the net power stored in the rotating assembly was assumed to be zero. Average specific work was obtained by integrating and averaging turbine power over five cycles and dividing by average turbine mass flow, as shown in Eq. 5.

$$\overline{W_s} = \frac{\overline{\dot{W}}_{turb}}{\overline{\dot{m}}_{turb,in}} \quad (5)$$

Rotor speed varied with time. Thus, time-accurate net shaft torque, $\tau_{shaft,net}$, was calculated using Eq. 6,

$$\tau_{shaft,net}(t) = I\left(\frac{\omega(t+\Delta t) - \omega(t)}{\Delta t}\right) \quad (6)$$

and rotational energy was calculated using Eq. 7.

$$KE_{rot}(t) = \tfrac{1}{2} I \left(\omega(t)\right)^2 \quad (7)$$

Turbine efficiency for conventional, steady turbines is the change in total enthalpy across the turbine divided by the ideal change in total enthalpy. A time-average formulation of unsteady turbine efficiency, which includes time-resolved measurement of temperatures, pressures, and velocities, must be integrated over an entire cycle. In this initial study, optical instrumentation emission detection threshold is 1300 K, limiting evaluation to the first 6 ms of blowdown. For this work, 1-D temperatures and velocities are measured at a single x-location, midway along the flowfield streamwise centerline. Only the x-component of velocity magnitude is reported. Figure 15 shows variation of turbine inlet velocity along the centerline at two moments in time: 0.174 ms after the detonation arrival and 3.306 ms after detonation arrival, respectively. Velocity varied by 200 m/s at 0.174 ms and by about 100 m/s at 3.306 ms.

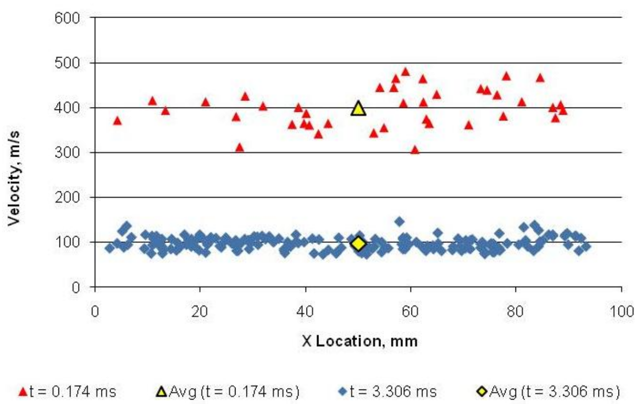

Figure 15. VARIATION IN VELOCITY AT TWO MOMENTS DURING BLOWDOWN.

Figure 16 shows turbine inlet static temperature variation in the y-direction at the streamwise mid x-location, approximately 610 mm upstream of the T3 turbine inlet flange. Temperature varied by 80 K at 0.174 ms and by nearly 300 K at 3.306 ms.

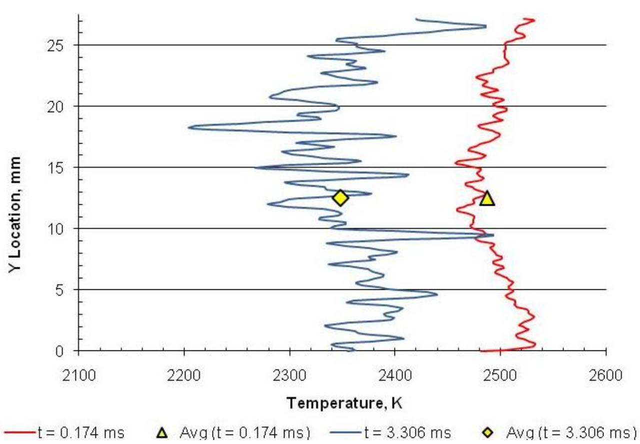

Figure 16. TURBINE INLET TEMPERATURE AT TWO MOMENTS DURING BLOWDOWN.

The ratio of hydrogen-air in the main fill was 0.03, by mass. Therefore, the ratio of specific heats, γ, was approximated using the gas constant for air and a fourth order curve fit for constant pressure specific heat for air over a range of temperatures. Thus, total temperature is obtained from static temperature and velocity:

$$T_t(t) = T(t) + \frac{V(t)^2}{2c_p} \tag{8}$$

Total pressure is obtained from static pressure, static temperature and velocity:

$$P_t(t) = P(t)\left(1 + \frac{V(t)^2}{2c_p T(t)}\right)^{\gamma/\gamma-1} \tag{9}$$

Because inlet and exit static temperature and velocity were measured at locations apart from inlet and exit static pressure, isentropic area relations were applied to account for varying area duct flow. On-going research includes a modified experimental arrangement which aligns pressure measurement locations with velocity and temperature.

Turbine mass flow rate is found from the Ideal Gas Law:

$$\dot{m}(t) = \frac{P(t)}{R \cdot T(t)} \cdot A \cdot V(t) \tag{11}$$

For this study, the optical instrumentation emission detection threshold of 1300 K limited measurement time to 6 ms, which is less than 10% of the total time for a complete PDC cycle: 66 ms. To evaluate efficiency, enthalpy is required for the entire cycle due to different characteristic times. This is apparent from a time-resolved energy formulation from the First Law of Thermodynamics:

$$\dot{H}(t)_{in} - \dot{H}(t)_{exit} = \dot{W}(t)_{turb} + \dot{E}(t)_{stored} + \dot{E}(t)_{loss} \tag{12}$$

where $\dot{E}(t)_{loss}$ is the rate at which energy is lost to the surroundings through mechanisms such as heat transfer.

Whereas most of the exhaust enthalpy is expected to arrive at the turbine inlet in a span of 6 ms, the turbine power output to the compressor is expected to endure for the entire cycle. For periodic operation, the net rotational energy stored over the entire cycle is expected to be zero. Therefore, this paper evaluates the time-average specific work output and time-resolved power and stored rotational energy over the entire cycle; however, time-resolved enthalpy is reported over 6 ms during blowdown. Until turbine inlet and exit enthalpy data is collected for an entire cycle, evaluation of time-average turbine efficiency is not possible.

FULL CYCLE PERFORMANCE RESULTS

Figure 17 shows a time history of rotor speed measured for 15 Hz, a fill fraction of 1.0 and a purge fraction of 0.5. Rotor speed was periodic over the three detonation cycles shown. Rise in rotor speed resulted from the detonation arrival at the turbine inlet and subsequent blowdown. Rotor speed dropped as blowdown ended, and continued falling through the purge phase while the combustion chamber pressure decreased. The fill phase momentarily decreased the rate at which rotor speed fell. The second sharp drop in rotor speed coincided with the end of the fill phase, at which time inlet valves closed, followed by ignition, then DDT, and then detonation propagation toward the turbine.

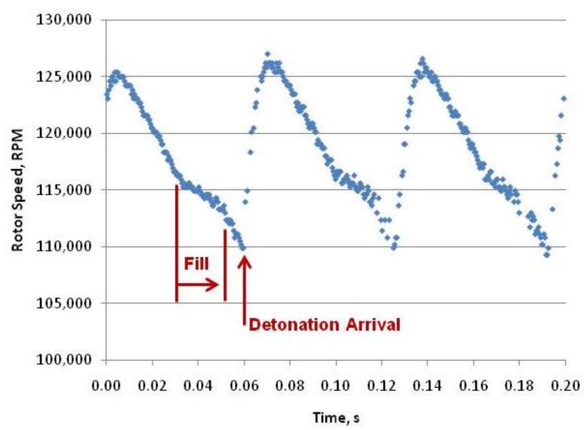

Figure 17. TIME HISTORY OF ROTOR SPEED FOR 15 HZ PDC, 1.0 FILL FRACTION AND 0.5 PURGE FRACTION.

Figure 18 shows time history of rotational energy, from Eq. 7, and net shaft torque, from Eq. 6, for one complete detonation cycle. From minimum rotor speed at the detonation arrival time to the time at peak rotor speed (about 11 ms), the average rate at which rotational energy was stored was 59.34 kJ/s (from the slope of the curve), and the average rate at which rotational energy was depleted over the remaining 55 ms was 11.57 kJ/s, from the time at peak rotor speed until the next detonation arrived. Torque response was dynamic, with a sharp increase that coincided with the rise in rotor speed. The ensuing large peaks and valleys in torque indicate possible winding and unwinding in the shaft. This ringing in the shaft was most pronounced during the rise in rotor speed but quickly settled as rotor speed began to fall.

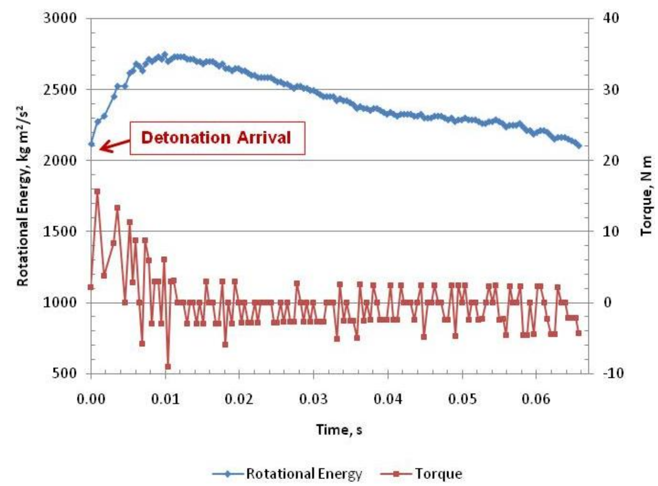

Figure 18. TIME HISTORY OF ROTATIONAL ENERGY AND NET SHAFT TORQUE FOR 15 HZ PDC, 1.0 FILL FRACTION AND 0.5 PURGE FRACTION.

Figure 19 shows time history of turbine power from compressor dynamometer measurements, and rotational energy stored in the rotating assembly, from Eq. 7 along with rotor speed measurements. The peak power lagged the peak rotational energy because the response of the compressor dynamometer is slower than that of the speed sensor. Peak power and peak rotational energy were both attained about 11 ms after their initial rise. Evaluations of time-averaged performance circumvent the phase shift between measurements.

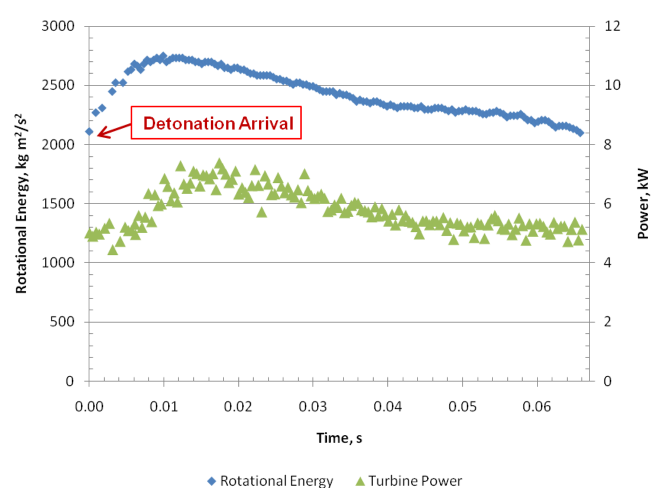

Figure 19. ROTATIONAL ENERGY AND POWER FOR 15 HZ PDC, 1.0 FILL FRACTION AND 0.5 PURGE FRACTION.

Full Cycle Time-Average Specific Turbine Work

Figure 20 includes instantaneous compressor dynamometer operating points overlaid on the manufacturer's map. The compressor dynamometer varied 15,000 RPM in corrected rotor speed. The red square represents the time-average point over a complete cycle, and most of the operation occurred within the 74% efficiency island.

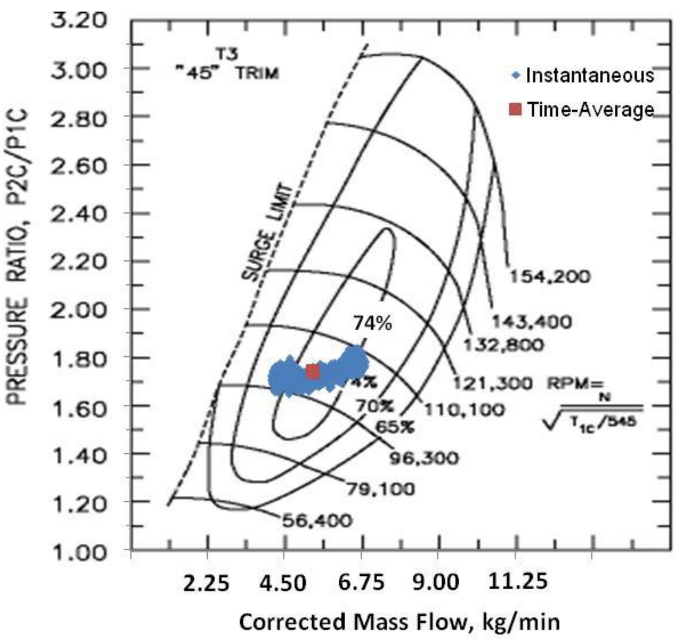

Figure 20. VARIATION IN CORRECTED ROTOR SPEED FOR 25 Hz PDC, 0.8 FILL FRACTION, AND 0.5 PURGE FRACTION.

Figure 21 shows consistent trends in average specific work as computed using Eq. 3, 4, and 5. Average specific work increases both with fill fraction and frequency. As shown in Table 1, main and purge manifold pressures also increases with fill fraction and frequency, as does average rotor speed. At 25 Hz, there is a 22% increase in main fill pressure from a fill fraction of 0.5 to 0.8, as shown in Table 1, and a 30% increase in average specific work. At a fill fraction of 0.8, there is a 21% increase in main fill pressure from 15 Hz to 25 Hz and an 80% increase in average specific work. Thus, specific work gains appear more sensitive to frequency than to main fill pressure (combustor inlet pressure). The sensitivity to frequency may also be linked to average rotor speed, which is the subject of on-going research.

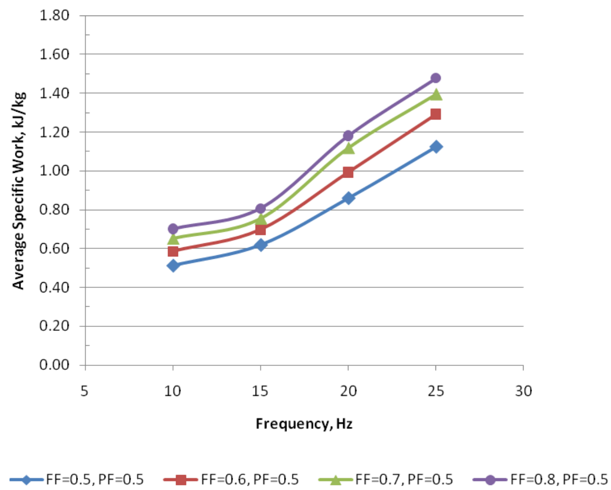

Figure 21. TIME-AVERAGE SPECIFIC TURBINE WORK FROM 10 HZ TO 25 HZ OPERATION, FILL FRACTIONS OF 0.5 TO 0.8, AND O.5 PURGE FRACTION.

TIME-RESOLVED TURBINE PERFORMANCE DURING BLOWDOWN

Time-resolved turbine performance was measured at 15 Hz, 1.0 fill fraction and 0.5 purge fraction. Figures 22 - 24 show time history of turbine inlet and exit pressure, temperature, and velocity, respectively, during a 6 ms portion of blowdown in the fire phase, in which the temperature is above the optical measurement threshold. The pressures, temperatures, and velocities were sampled at different frequencies; therefore, timing was synchronized by peak values associated with detonation arrival. Timing was determined by the temperature measurements taken at 0.087 ms intervals. Velocity measurements were taken at 0.067 ms intervals, and linear interpolation was used to synchronize with temperature in order to make calculations at the same moments in time. The interval for pressure measurements was 0.001 ms; therefore, no interpolation was required to obtain values at 0.087 ms intervals.

Figure 22 shows the time history of static pressure from the wall mounted transducers. The 14 mm transducer stand-off distance decreased the response, such that the expected C-J pressure peak was not captured during the first 0.5 ms. Expected C-J peak detonation pressure for hydrogen-air at these PDC operating conditions is approximately 2 MPa. Pressure profiles in the Taylor expansion that immediately trail a detonation are known to decay exponentially. Figure 22 possibly captured the latter part of the Taylor expansion at the turbine inlet and resolved the subsequent low frequency pressure behavior. The second rise in inlet pressure, at about 1.5 ms, is likely due to pressure waves reflecting off the turbine. Transient time between the initial rise in inlet and exit pressure was approximately 0.5 ms, which is used later when calculating unsteady storage of blowdown exhaust flow in the turbine.

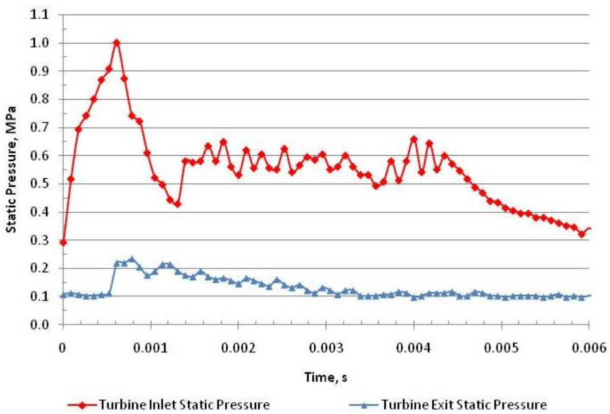

Figure 22. TURBINE INLET AND EXIT PRESSURE FOR 15 HZ PDC, 1.0 FILL FRACTION AND 0.5 PURGE FRACTION.

Figure 23 shows the time history of static temperature from the optical pyrometry measurements. Peak inlet temperature was near the expected C-J temperature for hydrogen-air at the PDC operating conditions: approximately 3,000 K. The inlet temperature dropped suddenly in the first 0.1 ms and maintained a plateau between 2,500 K and 2,000 K for more than 5 ms, followed by another sharp decline after 5 ms. The turbine exit static temperature was nearly constant over the first 5.5 ms. After 5.5 ms, the inlet temperature dropped faster than that of the exit. The inlet temperature fell below the 1300 K instrumentation threshold before the exit temperature, indicating that exit temperature exceeded inlet temperature between 5.5 ms and 6.0 ms.

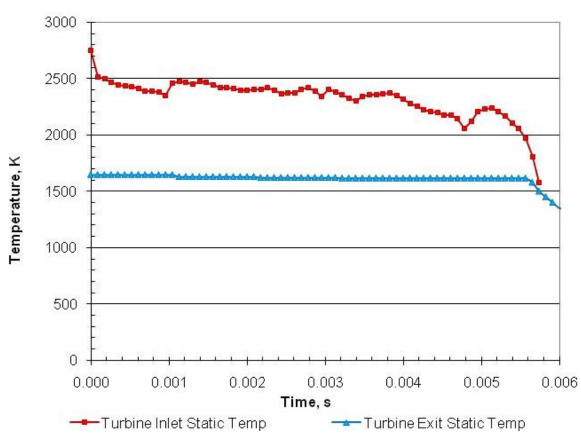

Figure 23. TURBINE INLET AND EXIT TEMPERATURE FOR 15 HZ PDC, 1.0 FILL FRACTION AND 0.5 PURGE FRACTION.

Figure 24 includes turbine inlet and exit velocity from PSV and BOS measurements. Peak inlet velocity associated with detonation arrival was near the expected C-J velocity for hydrogen-air at the PDC operating conditions; approximately 1,800 m/s. During the initial 0.6 ms, inlet velocity followed a decaying exponential function with an R^2 correlation coefficient of 0.95, indicating a good correlation to a Taylor wave. Negative velocity was observed at the inlet at about 1.5 ms, likely due to pressure waves reflecting off the turbine; however, velocity remained positive at the exit.

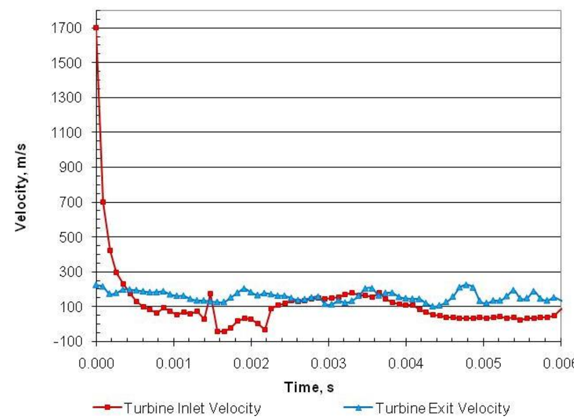

Figure 24. TURBINE INLET AND EXIT VELOCITY FOR 15 HZ PDC, 1.0 FILL FRACTION AND 0.5 PURGE FRACTION.

Figure 25 shows the time history of turbine inlet and exit mass flow rate over 6 ms of blowdown, using Eq. 11 and measurements of static pressure, static temperature, and velocity. The inlet mass flow rate oscillates above and below the exit mass flow rate, including periods of reverse flow observed at about 1.5 ms and 2.1 ms. Fluctuation in mass storage is indicative of unsteady turbine performance. Due to periodic turbine operation, as noted in Fig. 17, there is expected to be no net storage of mass over the entire PDC cycle.

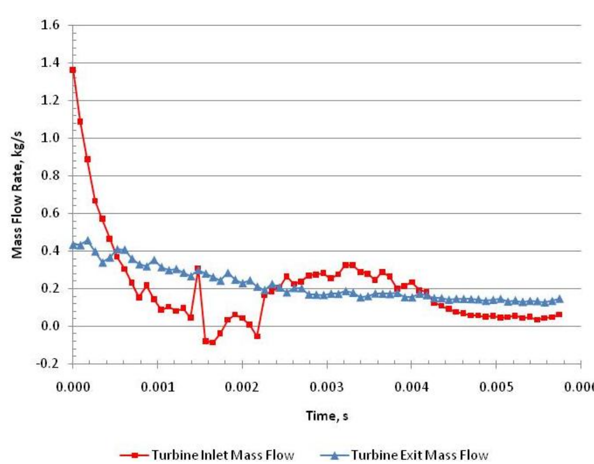

Figure 25. TURBINE INLET AND EXIT MASS FLOW RATE FOR 15 HZ PDC, 1.0 FILL FRACTION AND 0.5 PURGE FRACTION.

Figure 26 shows time history of turbine inlet and exit enthalpy over 6 ms of blowdown. Enthalpy flowed into the turbine at a higher rate than at the exit for most of the 6 ms interval. The initial spike in enthalpy is related to the peak temperature and velocity, which included peak C-J values for hydrogen-air. Future calculations for turbine efficiency will require enthalpy measurements for the entire PDC cycle.

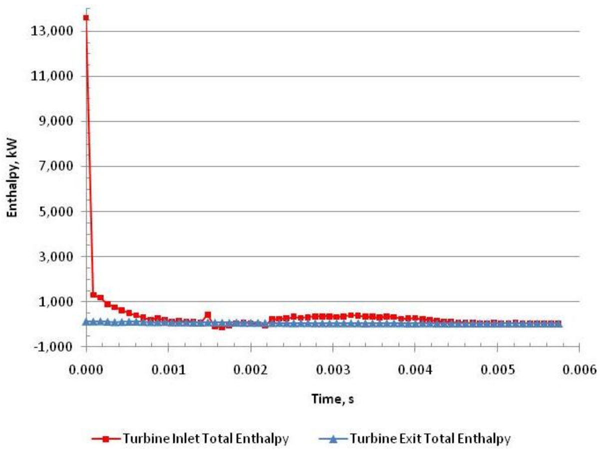

Figure 26. TURBINE TOTAL ENTHALPY FLOW FOR 15 HZ PDC, 1.0 FILL FRACTION AND 0.5 PURGE FRACTION.

CONCLUSIONS

This paper evaluated unsteady performance of a turbine driven by pulsed detonations, in terms of time-average specific work and time-resolved rotor speed, rotational energy, torque, power and turbine inlet and exit enthalpy. Average specific work was assessed over a range of PDC operating conditions, increasing with frequency and demonstrating more sensitivity to frequency than main fill pressure. Time-resolved performance was evaluated at a single operating condition: 15 Hz PDC, 1.0 fill fraction, and 0.5 purge fraction. Time-resolved rotor speed response was shown to be periodic. Rotational energy was stored at an average rate of 59.34 kW, and torque measurements indicated an oscillating twist in the shaft response to the detonation, with a peak net shaft torque of 16 N m. Peak shaft power and rotational energy were achieved within 11 ms of initial turbine response to the detonation arrival. Turbine inlet and exit flowfield measurements were limited by the emission threshold of the optical measurements, capturing the first 0.6 ms of blowdown. Inlet mass flow included momentary reverse flow; however, reverse flow was not observed at the turbine exit. Therefore, in order to evaluate time-average turbine efficiency, enthalpy measurements are required for the entire PDC cycle, which is the subject of on-going research.

NOMENCLATURE

A = Area, m^2
c_p = Specific heat at constant pressure, J kg/K
$\bar{c}_p$ = Average specific heat at constant pressure, J kg/K
E = Energy, J
H_t = Total enthalpy, N m
I = Moment of inertia, kg m^2 (3.2E-5 kg m^2)
m_{cum} = Cumulative mass
$\dot{m}$ = Mass flow, kg/s
$\dot{m}_{compr}$ = Compressor mass flow, kg/s
$\dot{m}_{turb}$ = Turbine mass flow, kg/s
$\overline{\dot{m}}_{turb}$ = Time-average turbine mass flow, kg/s
KE_{Rot} = Rotational energy, kg m^2/s^2
P = Static pressure, Pa
P_t = Total pressure, Pa
R = Gas constant, J/kg K
T = Static Temperature, deg K
T_t = Total temperature, deg K
t = Time, s
u = Axial velocity, m/s
V = Velocity, m/s
$\forall$ = Volume, m^3
$\dot{\forall}$ = Volumetric flow rate, m^3/s
$\dot{W}_{turb}$ = Turbine power, kW
$\overline{\dot{W}}_{turb}$ = Time-average turbine power, kW
W_s = Specific work, J/kg/s
$\overline{W}_s$ = Time-average specific work, Watts/kg/s
Δt = Time interval
φ = Equivalence ratio
γ = Ratio of specific heats
$\bar{\eta}_{compr}$ = Time-average compressor efficiency
$\bar{\eta}_{mech}$ = Time-average mechanical efficiency
ω = Rotor speed, rad/s (RPM)
$\tau_{shaft,net}$ = Net shaft torque, N m

Abbreviations

AFRL = Air Force Research Laboratory
BOS = Background Oriented Schlieren
C-J = Chapman-Jouguet
CPC = Constant Pressure Combustor
DDT = Deflagration to Detonation Transition
DERF = Detonation Engine Research Facility
FF = Fill Fraction

LED = Light-Emitting Diode
MAF = Mass Air Flow
PDC = Pulsed Detonation Combustor
PDE = Pulsed Detonation Engine
PF = Purge Fraction
PIV = Particle Image Velocimetry
PSV = Particle Streak Velocimetry
RPM = Revolutions Per Minute
SiC = Silcon Carbide
UC = University of Cincinnati

ACKNOWLEDGMENTS

The authors thank the Detonation Engine Research Facility team for technical and fabrication support that made this research possible, especially Chris Stevens, Andy Naples, Curtis Rice, David Burris, and Justin Goffena. Special thanks is due to Larry and Cory Goss for instrumentation support. Appreciation is also expressed to Dr. Robert Hancock (AFRL/RZT), Dr. Joseph Zelina (AFRL/RZTC), and Dr. Charles Stevens (AFRL/RZTT) for their technical leadership. Funding was provided by the Air Force Research Laboratory, Propulsion Directorate and AFOSR.

REFERENCES

[1] Heiser, William H., and Pratt, David T., "Thermodynamic Cycle Analysis of Pulse Detonation Engines," AIAA Journal of Propulsion and Power, Vol. 18, No. 1, Feb 2002.

[2] Bussing, T., and Pappas, G., "An Introduction to Pulse Detonation Engines," AIAA 94-0263, 32nd AIAA Aerospace Sciences Meeting, Jan 1994.

[3] Dyer, R.S., and Kaemming, T.A., "The Thermodynamic Basis of Pulsed Detonation Engine Thrust Production," AIAA 2002-4072, 38th AIAA/ASME/SAE/ASEE Joint Propulsion Conference, July 2002.

[4] Hoke, John, Bradley, Royce, Stutrud, Jeffrey, and Schauer, Fred, "Integration of a pulsed detonation engine with an ejector pump and with a turbo-charger as methods to self-aspirate," 40th AIAA Aerospace Sciences Meeting, AIAA 2002-0615, Jan 2002.

[5] Schauer, Fred, Bradley, Royce, and Hoke, John, "Interaction of a Pulsed Detonation Engine with a Turbine," 41st AIAA Aerospace Sciences Meeting, AIAA 2003-0891, Jan 2003.

[6] Glaser, A., Caldwell, N., Gutmark, E., "Performance Measurements of a Pulse Detonation Combustor Array Integrated with an Axial Flow Turbine," AIAA 2006-1232, 44th AIAA Aerospace Sciences Meeting, Jan 2006.

[7] Caldwell, N., Glaser, A., Gutmark, E., "Performance Measurements of a Pulse Detonation Engine Array Integrated with a Turbine," AIAA2006-4307, 42nd AIAA/ASME/SAE/ASEE Joint Propulsion Conference, July 2006.

[8] Caldwell, N., Gutmark, E., "Performance Analysis of a Hybrid Pulse Detonation Combustor/Gas Turbine System," AIAA 2008-4880, 44th AIAA/ASME/SAE/ASEE Joint Propulsion Conference, July 2008.

[9] Rouser, K., King P., Schauer, F., Sondergaard, R., Hoke, J., "Unsteady Performance of a Turbine Driven by a Pulse Detonation Engine," AIAA 2010-1116, 48th AIAA Aerospace Sciences Meeting, Jan 2010.

[10] Rouser, K., King P., Schauer, F., Sondergaard, R., Hoke, J., "Parametric Study of Unsteady Turbine Performance Driven by a Pulse Detonation Combustor," AIAA 2010-6536, 46th AIAA/ASME/SAE/ASEE Joint Propulsion Conference, July 2010.